




## 20 Abstract

21 Rapid-response petrological monitoring is a major advance for volcano observatories to build and validate  
22 models in near-real-time of the plumbing systems that supply eruptions. Our rapid-response analysis of tephra from  
23 the September 2023 eruption of Kīlauea shows that Raman analyses of fluid inclusions can robustly determine  
24 magma reservoir depths within a day of receiving samples – a transformative timescale for decision making that  
25 has never been achieved by petrological methods.



## 27 Main text

28 Volcano observatories increasingly use data collected from erupted lava and tephra samples in near-real-  
29 time to obtain information about the magmatic plumbing system to help inform decision making during volcanic  
30 crises<sup>1–3</sup>. Most work so far has focused on the chemistry of erupted lavas and crystal cargoes<sup>3</sup> to gain insight into  
31 changing melt composition and rheological properties (e.g., ref<sup>1</sup>). However, up until now, petrological monitoring  
32 has been unable to address the high-priority question– ‘*Where is the magma coming from?*’<sup>2</sup>. At well-monitored  
33 volcanoes, such information can be used to draw analogies to previous eruptive episodes associated with specific  
34 storage reservoirs (e.g., vigour, pathway, or length of eruption), and to help interpret geophysical signals of ongoing  
35 activity. At poorly-monitored volcanoes, where there may be no prior constraints on magma storage geometry<sup>4</sup>,  
36 depths of storage are a vital parameter to begin interpreting new eruptive activity. Melt inclusion (MI) barometry,  
37 a widely popular petrological method to determine storage depths from volatile contents, takes months to years to  
38 complete<sup>2</sup>. While mineral barometry could be implemented faster (only requiring electron probe microanalysis  
39 (EPMA) measurements on eruptive minerals), it is imprecise<sup>5,6</sup>, and therefore would only be able to constrain  
40 magma storage to very broad depths (e.g., stored in the crust vs. below the Moho). This technique has particularly

41 poor applicability at active volcanoes such as Kīlauea or Mauna Loa, where a precision of 1–2 km is needed to  
42 distinguish between storage reservoirs<sup>7,8</sup>.

43 Recent developments have shown that Raman-based barometry of CO<sub>2</sub>-rich fluid inclusions (FI) provides  
44 an  exciting alternative to popular petrological barometers, with much smaller uncertainties than mineral barometry,  
45 and requiring far less time and resources than MI analyses<sup>9,10</sup>. This method uses spectral features of CO<sub>2</sub> fluids to  
46 calculate a CO<sub>2</sub> density using an instrument specific calibration<sup>11</sup>. Along with an estimate of entrapment  
47 temperature, this density is converted into an entrapment pressure using a CO<sub>2</sub> Equation of State (EOS). Pressures  
48 are converted to depths through an estimate of crustal density. However, there has previously been no rigorous  
49 assessment of ~~just~~ how quickly FI depths can be obtained from erupted material, and whether these timescales are  
50 short enough to have use as a real-time monitoring tool.

51 The eruption onset of Kīlauea volcano on September 10, 2023 provided an unprecedented opportunity to  
52 test the validity of this method during a response, given that depths of the main magma storage regions at this  
53 volcano have been well constrained by various independent geophysical and petrological methods, including prior  
54 FI barometry<sup>10</sup>. Tephra samples representing the first ~14 hours of the September 2023 eruption were collected by  
55 Hawaiian Volcano Observatory (HVO) geologists on September 12. ~~Following discussions with HVO over the~~  
56 ~~next few days, we requested samples to run a rapid-response simulation.~~

57 Our simulation started on September 20 at 9 am PST (Day 1) ~~following receipt of samples the day before~~  
58 (Fig. 1). We used a production-line style workflow involving two undergraduates, a 1<sup>st</sup> year graduate student, a  
59 post-doc, and an assistant professor, with stations for crushing and sieving, mineral picking, FI preparation, sample  
60 cataloguing, and analysis. The first steps were to crush and sieve tephra, pick olivine crystals (size fractions 0.5-1  
61 and 1-2 mm) crystals, and begin mounting crystals in CrystalBond<sup>TM</sup>  to search for FI. By 2 pm PST (5 hrs into the  
62 simulation), we had collected our first Raman spectra. By ~7 pm PST, we had analysed and processed all data for  
63  FI and were able to share a histogram of storage depths with HVO collaborators showing that crystals, and thus

64 magma, were coming from the shallower Halema'uma'u reservoir of Kīlauea (HMM on Fig. 2a–b). We also had a  
65 further ~20 FI fully prepared and catalogued for analysis. On Day 2, these 20 FI were analysed, while further FI  
66 were prepared and catalogued. After analysis of ~15 crystals hosting FI, these crystals were passed from the Raman  
67 to a workstation where they were removed from CrystalBond™ and placed on tape to make an epoxy mount. Epoxy  
68 was poured at the end of the day. By ~8:30 pm PST on Day 2, we shared an updated histogram of 46 FI pressures  
69 and depths, confirming the dominant influence of the Halema'uma'u reservoir (Fig. 2a and c). On Day 3, while  
70 waiting for the epoxy to fully set, we finished analysing prepared FI. Then we polished the mount and began  
71 cataloguing the regions of crystals on which to perform energy-dispersive spectroscopy (EDS). On Day 4, olivine  
72 forsterite contents ( $Fo = 100 * Mg / (Mg + Fe)$  molar) were determined by EDS, providing a framework to further  
73 interpret the plumbing system (Fig. 2d).

74 Our results clearly show that the majority of FI were entrapped at ~1–2 km below the surface (Fig. 2d),  
75 which aligns well with the depths of the Halema'uma'u reservoir interpreted from geophysics<sup>7,8,12</sup>, MI barometry  
76 <sup>13,14</sup>, and FI barometry<sup>10</sup>. While the greater number of analyses from data processed on Day 2 and Day 4 certainly  
77 enhance the story, it is notable that depths calculated on Day 1 fall within final proposed storage reservoir depths  
78 as well. Rapid EDS analyses of olivine Fo contents close to each FI reveal that olivine crystals grew from a wide  
79 range of melt compositions. It is interesting to note that FI in the cores of high-Fo (e.g., >86) olivine crystals return  
80 pressures indicative of the shallower Halema'uma'u reservoir – it has been suggested in previous eruptions that  
81 these high-Fo olivine crystals predominantly grow in the deeper South Caldera reservoir (SC on Fig. 2a), where  
82 high MgO melts are thought to reside. We suggest three possible scenarios to explain the relatively shallow  
83 pressures documented in high-Fo olivine crystals:

84 1) FI in high-Fo olivine crystals were entrapped within the South Caldera reservoir and re-equilibrated at  
85 Halema'uma'u pressures prior to eruption.

86 2) High-MgO melts were injected into the Halema'uma'u reservoir, where high-Fo olivine crystallized and trapped  
87 FI.  
88 3) Complex skeletal growth of olivine crystals during extensive undercooling (e.g., ref <sup>15</sup>) meant that high-Fo  
89 olivine cores which initially grew in the South Caldera reservoir texturally evolved and trapped lower pressure FI  
90 in the Halema'uma'u reservoir.

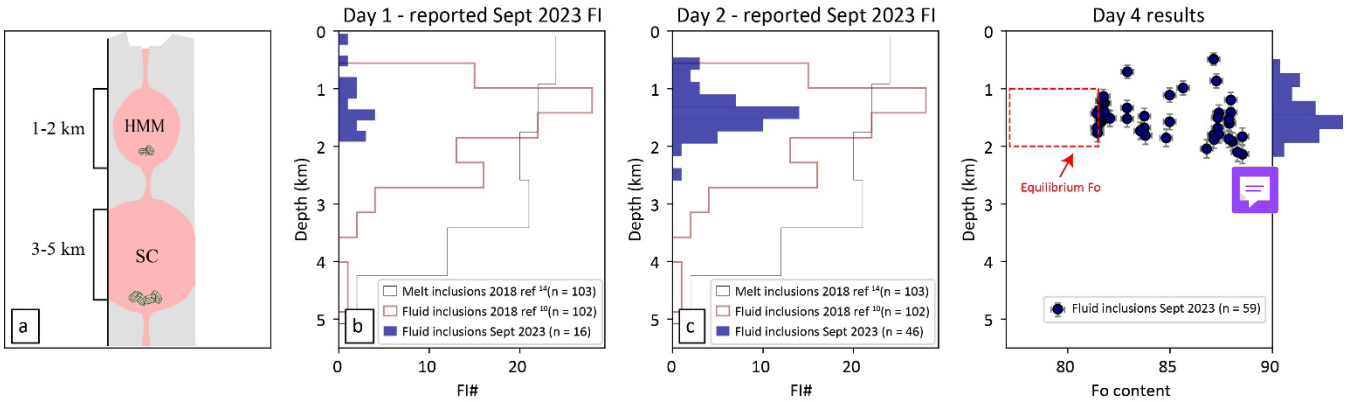
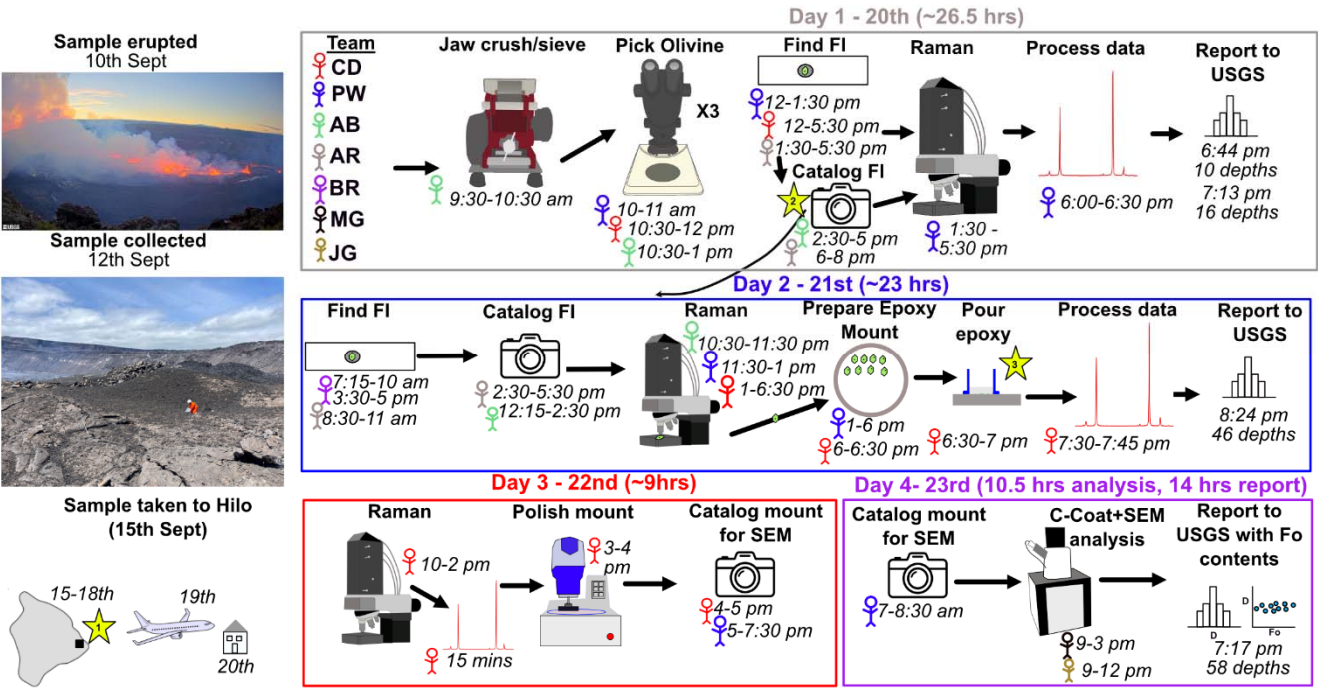
91 We think that scenario 1 is unlikely given the that FI from the 2018 lower East Rift Zone eruption appear  
92 not to have re-equilibrated despite stalling in the Halema'uma'u reservoir for up to 2 years<sup>10,16</sup>, and our models of  
93 FI re-equilibration indicate <10% change in pressure after such a period. Current data does not allow us to resolve  
94 scenario 2 vs 3, but this eruption could provide an opportunity to explore this further (e.g., through detailed  
95 Phosphorous mapping in olivine around FI). Regardless of the exact mechanism, our FI pressures indicate that  
96 erupted crystal cargo experienced storage in the Halema'uma'u reservoir prior to eruption, and thus this is the most  
97 probable reservoir supplying magma to the surface.

98 This simulation shows that Raman-based FI barometry has significant potential for rapid-response  
99 petrological monitoring globally. It could be applied to any CO<sub>2</sub>-rich volcanic system – which includes numerous  
100 hazardous and frequently active volcanic regions worldwide (e.g., Galápagos, Réunion, Azores, Canary Islands,  
101 Iceland, Cabo Verde). The resources and personnel required are modest. Sample preparation was carried out using  
102 transmitted-reflected light microscopes from the University of California teaching collection, only using a research-  
103 grade microscope for sample cataloguing. Raman spectrometers are widely available at many universities, given  
104 that it is a popular technique in many other fields, such as material sciences, physics, chemistry, and biology, and  
105 the W-filament SEM used for EDS analyses to get olivine Fo contents has been around for 15 years (See Methods).

106 This simulation also enabled us to identify several 'bottlenecks' in this rapid-response workflow which  
107 could be smoothed out during future eruptions (yellow stars, Fig 1):

- 1) No courier services ship packages out of Hilo, Hawai‘i over the weekend, and estimated delivery days are not reliable.
- 2) The epoxy took 18 hours to cure enough for polishing (vs. 8 hours on the datasheet)
- 3) We spent significant time cataloguing samples on a research-grade microscope to help navigate on the Raman, but later realized that smartphone cameras with teaching microscopes would have worked faster.

Overall, we have demonstrated that a modest-sized research group with prior teaching and class commitments working without overnight shifts can obtain pressures on ~~game-changing~~ timelines for understanding volcanic plumbing systems during periods of unrest. This technique adds valuable quantitative storage depth information that expands on HVO’s routine near-real-time chemical monitoring with bulk rock ED-XRF<sup>1</sup>. In a true eruptive crisis, magma storage depths could be obtained even faster by removing bottlenecks 1–3, implementing overnight shift work, and requesting teaching release and class absences for students.



127 **Figure 2: Evolution of results over 4 days.** a) Schematic model of Kīlauea's plumbing system, indicating reservoir  
128 depths determined by geophysics and prior petrological work (HMM- Halema'uma'u; SC – South Caldera). b) By  
129 the end of Day 1, FI revealed that the crystals were supplied from the Halema'uma'u reservoir. KS tests show that  
130 within 5% confidence this is significantly shallower than depths indicated by FI (critical  $D = 0.22$ ,  $\text{stat} = 0.24$ ,  
131  $p\text{val}=0.016$ ) and MI (critical  $D = 0.22$ ,  $\text{stat} = 0.41$ ,  $p\text{val}=3.51\text{e-}06$ ) from the 2018 lower East Rift Zone eruption,  
132 which required a contribution from the South Caldera reservoir. c) By the end of Day 2, depths from 46 FI were  
133 sent to HVO, confirming a very dominant role of the Halema'uma'u reservoir. On Day 2 we applied a conservative  
134 degassing filter ( $\text{SO}_2 \text{ mol\%} < 2.5$ ). d) By the end of Day 4, after taking a mean of repeated analyses of single FI,  
135 applying more stringent data filters, using FI-specific temperatures, and a more appropriate crustal model (density  
136 of  $\sim 2300 \text{ kg/m}^3$  with a normal error distribution of  $100 \text{ kg/m}^3$ ), entrapment depths with uncertainties were linked  
137 to crystal chemistry. Olivine Fo equilibrium field is calculated based on Glass EPMA data (see Methods). We note  
138 here that initial data for Days 1 and 2 did not filter out repeated analyses (1 repeated FI in Day 1 and 6 in Day 2),  
139 pressures were calculated using an estimated entrapment temperature of  $1150^\circ\text{C}$ , and depth was calculated using  
140 the model of ref<sup>17</sup> described in ref<sup>13</sup> for crustal density.

141

## 142 **Methods (Online)**

### 143 **Sample collection and preparation**

144 Tephra samples (USGS code KS23-588) representing the first  $\sim 14$  hours of the September 10, 2023,  
145 eruption of Kīlauea volcano were collected by Hawaiian Volcano Observatory (HVO) geologists on September 12  
146 and shipped on Friday September 15 at  $\sim 5$  pm HST. This tephra was erupted from a fissure which opened at 15:36  
147 local time on September 10 ( $\sim 22$  minutes after the eruption started, between 15:13 and 15:14 local time) and ceased  
148 erupting between 06:16 and 06:18 am local time on September 11. Following receipt of the samples at the  
149 University of California, Berkeley on Tuesday, September 19, material was processed in a jaw crusher, and then



150 sieved into >2 mm, 1–2 mm, and 0.5–1 mm size fraction. Crystals were picked from the 1–2 mm and 0.5–1 mm  
151 size fractions using three different binocular microscopes (one of which had the ability to cross polars). Then,  
152 crystals were individually mounted in CrystalBond™ on glass slides and progressively polished with 1200-2500-  
153 10000 grade wet and dry paper to find FI. FI were then passed onto a team member on a research grade scope to  
154 take reflected and transmitted light images to aid with Raman navigation. These images were pasted into a Google  
155 slides document so all lab personnel at UC could access them immediately.

156 Glass compositions were measured on USGS sample KS23-587, a lava flow sample collected in a molten  
157 state and quenched with water at 06:30 HST on 11 September 2023. The sample was entirely glassy, and fragments  
158 were mounted in epoxy in a 1” round and polished for microprobe analysis.

159

160

## 161 Raman analyses

162 Raman spectra were acquired using a WiTec Alpha 300R Raman spectrometer at the Department of Earth  
163 and Planetary Science at the University of California, Berkeley. The relationship between CO<sub>2</sub> density and spectral  
164 features was determined from a gas calibration cell following the methods of ref<sup>10</sup>. All spectra were acquired at 37  
165 °C. Spectra were processed and corrected for drift using the Python tool DiadFit v0.0.73<sup>18</sup>. We report ratios of SO<sub>2</sub>  
166 and CO<sub>3</sub> to CO<sub>2</sub> peak areas and calculate approximate mol % SO<sub>2</sub> using the equations of ref<sup>19</sup>, implemented in  
167 DiadFit. All measured FI had SO<sub>2</sub> mol % <10, we filtered the final dataset for SO<sub>2</sub> mol % <5 (Fig. 2d), to ensure  
168 use of the pure CO<sub>2</sub> EOS was valid. We calculated densities from the Raman-measured separation of the Fermi  
169 diad using the appropriate calibrated density equations for our instrument in DiadFit<sup>18</sup>. We then calculated pressures  
170 using the EOS of ref<sup>20</sup> and an entrapment temperature estimated from the Fo content<sup>10</sup>. We propagated uncertainties  
171 in FI depths using MonteCarlo simulations implemented in DiadFit. Entrapment depths in Fig. 2d were calculated  
172 using a constant crustal density of 2300 kg/m<sup>3</sup> and a normally distributed 1σ error of 100 kg/m<sup>3</sup>. Error in the CO<sub>2</sub>

173 density for each FI was determined from the error in each peak fit, the Ne line drift correction model, and the  
174 densitometer<sup>18</sup>. We used a 40°C error for temperature. In total we analyzed 62 FI hosted in 31 olivine crystals. Our  
175 workflow is detailed in Fig. 1. Pictures of each FI and host crystal are available in the supplement (Image  
176 Compilation S2).

177

## 178 **Epoxy mount making and polishing**

179 After Raman analysis, crystals were removed from CrystalBond<sup>TM</sup> using a hotplate and placed in Acetone.  
180 They were then mounted on double-sided sticky tape with their polished side down. EpoFix<sup>TM</sup> resin was used to  
181 impregnate the samples in a Cast-N-Vac vacuum pourer. After curing, the epoxy mount was polished using an  
182 EcoMet30 automatic polisher, with 9, 3, and 1  $\mu\text{m}$  diamond pastes. A reflected light map and image of each crystal  
183 was taken using the Raman microscope to aid SEM sample navigation. The location within each FI within the  
184 reflected light image was cataloged so the Scanning Electron Microscope (SEM) operator knew where to analyze  
185 to obtain an approximate Fo content for each FI.

186

## 187 **EDS analysis**

188 Samples were carbon coated to an approximate thickness of 25–30  $\mu\text{m}$  for EDS analysis. Chemical data  
189 for each host crystal in the proximity of each FI was determined using a Zeiss EVO MA-10 SEM and a single  
190 AMETEK EDAX 10  $\text{mm}^2$  detector at the University of California, Berkeley. The beam was rastered over a 30-by-  
191 30  $\mu\text{m}$  area for ~75–80s (a live time of 60 seconds with ~30% dead time). For all analyses we used an accelerating  
192 voltage of 20 kV and a 30  $\mu\text{m}$  aperture, giving an approximate beam current of 5 nA. EDS data reduction was  
193 performed using an in-built standardless quantification routine (including a ZAF matrix correction), alongside pre-  
194 determined “Standardless Element Coefficients” (SECs). The SECs act as correction factors for each element in  
195 the standardless quantification routine and have been determined through several years of repeat analyses of

multiple different silicate standard materials and glasses. This method returns an estimate for the relative abundance of each element in the analyzed material and, if a normalization to 100% is assumed, can be used to return semi-quantitative chemical analysis of elemental or oxide weight percent values. However, for the purposes of this study we simply focused on the relative abundance of Mg and Fe in the EDS analyses to calculate the Fo content of the olivine host crystals. Furthermore, by calculating the molar Si/(Mg+Fe) ratio of each analysis we were able to provide a stoichiometric check of data quality: we obtained an average Si/(Mg+Fe) ratio of  $0.497 \pm 0.006$  on Kīlauea olivine crystals, close to the ideal value of  $\sim 0.5$ . Precision and accuracy were determined through repeat measurements of the San Carlos and Springwater olivines, which were not used as part of the standard quantification routine. We estimate the precision and accuracy of the method using repeat analyses of secondary standards (5 at start, 5 at end of day), which have Fo contents similar to our samples (see supplementary dataset S1). The Smithsonian-preferred Fo content<sup>21</sup> for the San Carlos secondary standard is 90.2 Fo, and we obtained a mean of  $89.84 \pm 0.07$  Fo units. For Springwater, the preferred value is 82.4 Fo, and we obtained a mean of  $82.1 \pm 0.2$  Fo. We also analyzed a Kīlauea olivine crystal previously measured on the USGS Menlo Park EPMA. The average Fo content obtained at Menlo Park was  $87.8 \pm 0.1$  Fo units, and at the University of California, Berkeley SEM,  $88.5 \pm 0.1$ . It should be noted that such offsets also exist between different EPMA labs<sup>5</sup>. Considering these probable differences, we compared data acquired at Stanford University to that obtained at Cambridge University on the olivine crystals of ref<sup>14</sup>. The difference observed amounts to  $\sim 0.62$  units at  $\sim 82$  Fo and 0.78 units at 90 Fo<sup>10</sup>.

213

214 **EPMA analysis of glasses**

Major and minor element analysis of glass from a 11 September 2023 lava (sampled molten, water quenched) was done using the U.S. Geological Survey's JEOL 8530F microprobe at the California Volcano Observatory. Analyses used 15 kV accelerating voltage and a 10  $\mu\text{m}$  beam with a 10 nA current. Peak counting times were 45 s for S, Cl, and F, 40 s for Ti, P, and Mn, 20 s for Si, Ca, Fe, Al, and Mg, and 10 s Na and K

219 (backgrounds were measured on both sides of the peak for half the peak counting times). Standards for glass  
220 analyses were VG2 basaltic glass (USNM 111240/52;ref<sup>21</sup>) for Si, Mg, and Al, Kakanui Pyrope Garnet (USNM  
221 143968) for Fe, and Al, Wollastonite for Ca, Tiburon Albite for Na, MnO<sub>3</sub> for Mn, TiO<sub>2</sub> for Ti, Orthoclase OR-1A  
222 for K, Wilburforce Apatite (USGS-M105731) for P, Barite for S, Sodalite for Cl, and MgF<sub>2</sub> for F. Two-sigma  
223 relative precision, based on two analyses of VG-2 glass (before and after lava sample was run), are 0.19 wt% for  
224 SiO<sub>2</sub>, 0.15 wt% for Al<sub>2</sub>O<sub>3</sub>, 0.003 wt% for TiO<sub>2</sub>, 0.27 wt% for FeO, 0.009 wt% for MnO, 0.006 wt% for MgO, 0.04  
225 wt% for CaO, 0.11 wt% for Na<sub>2</sub>O, 0.02 for K<sub>2</sub>O, 0.04 for P<sub>2</sub>O<sub>5</sub>, 0.07 for SO<sub>3</sub>, 0.0001 for Cl, and 0.002 for F. X-ray  
226 intensities were converted to concentrations using standard ZAF corrections<sup>22</sup>. Analyses with totals <99.0 wt% or  
227 >100.5 wt% were rejected. Reported analyses are an average of four replicate points on individual glass fragments.

228

## 229 **Identifying and Resolving Bottlenecks**

230 The yellow stars on Fig. 1 identify current bottlenecks in the process that could be easily improved.

231

### 232 ***Star 1 - Shipping and receiving samples***

233 Distributing samples to the University of California, Berkeley was not a top priority for HVO because this  
234 simulation was being attempted for the first time, and as a result, there was no guarantee of obtaining magma  
235 storage depths in a timely manner. Samples were shipped from Hilo on a Friday at ~5 pm HST. HVO was asked to  
236 ship samples to a private residence under the assumption that they might arrive over the weekend. However, no  
237 packages leave Hilo after 4pm on Friday over the weekend, so the samples started their transit to California on  
238 Monday. Had the package been taken to the courier's office on Friday morning, it would likely have arrived on  
239 Sunday. The tracking information indicated arrival on Wednesday, which is when we planned to start the  
240 simulation. However, the samples arrived at the private residence on Tuesday morning during working hours,  
241 without notification that the package had been delivered (and no one was home).

242 We have demonstrated that this technique adds valuable quantitative depth information that expands on  
243 HVO's routine near-real-time chemical monitoring with bulk rock ED-XRF<sup>1</sup>. Under ideal circumstances, HVO  
244 geologists would sample tephra or molten lava from the eruption on Day 1 (morning) and dry the samples in the  
245 lab on Day 1 (afternoon), dropping the samples for shipment on the evening of Day 1, which would go out early  
246 on Day 2 (as long as the drop off did not occur Friday afternoon or over the weekend). Same-day shipping from  
247 Hawaii to California is not realistic, but samples shipping Monday through Thursday mornings would allow for  
248 arrival on Day 3. Additionally, it would be possible to get samples to the University of California, Berkeley within  
249 24 hours if someone in Hawai'i were to take a flight to San Francisco or Oakland airport with the samples, or within  
250 ~30 hours if someone based in the University of California, Berkeley flew to Hawai'i, picked up the samples, and  
251 returned home immediately.

252 We note that this bottleneck can be avoided entirely if observatories rely on local research expertise (for  
253 example, in collaboration with local academic research groups) and/or establish in-house workflows for this type  
254 of work. In such a case, next-day information could readily be obtained. As this is not an option for HVO, the  
255 Hawaii-California connection will serve as the fastest way to conduct this rapid-response barometry.

256

## 257 *Star 2 – Sample cataloging*

258 The WITEC Raman microscope used in this study does not have a condenser in its optical path, which can  
259 make it very hard to navigate and find FIs, particularly in volcanic crystals that are commonly coated in glass. The  
260 first 7–10 crystals were analyzed immediately after preparation, so navigation took some time. After AB had  
261 finished crushing, sieving, and picking, he began taking photos on a research-grade scope to help the Raman  
262 operator find the FIs they were supposed to be analyzing. Late on Day 2, when students were not available, Wieser  
263 began photographing crystals holding her phone to the eyepiece of the teaching-collection reflected light and  
264 transmitted light microscopes. This provided enough textural context to easily find FIs on the Raman (Fig. S1 and

265 S2). The main advantage of using smartphones is that the person who found each FI could identify it, rather than  
266 passing it off to another person who then must work out where the FI is before photographing it. This would greatly  
267 reduce the number of people involved, as we almost always had one person taking photos.

268

269 ***Star 3 – Epoxy impregnation***

270 We used EpoFix™ epoxy, which is what was available in our lab (chosen because it gives low backgrounds  
271 during SIMS analysis). After pouring the epoxy at ~7 pm, it was removed from its mount at ~9 am the next morning.  
272 The epoxy was still noticeably soft (to the extent it cracked coming out of the mold). This meant that we could not  
273 start polishing immediately. Instead, we had to wait a further ~5 hours for it to cure sufficiently to polish. If fast-  
274 curing epoxies were available, it is very possible that a team member could have stayed, and polished and cataloged  
275 the sample overnight, allowing SEM analysis on Friday (Day 3) rather than Saturday.

276

277 **Author contributions**

278 Author contributions for lab work are shown on Fig. 1. CD and PW wrote the paper. CD, PW, AR, BR,  
279 and AB prepared tephra, picked olivine, found FIs, catalogued them, mounted them, and Raman-ed them. CD and  
280 PW performed all spectral fitting, data processing, and figure making, with schematic illustrations shown in Fig. 1  
281 from AB. JG developed the Mg/Fe calibration for the EDS detector and MG performed EDS analyses with help  
282 from JG. KJL, DTD, NID and KMM collected samples, processed them in Hilo, and provided eruption context.  
283 KJL and DD prepared the glass mount and did the EMPA analyses.

284

285 **Acknowledgements**

PW and CD acknowledge support from NSF EAR 2217371 and the Berkeley Rose Hills Innovator Program. Any use of trade, product, or firm names is for descriptive purposes only and does not imply endorsement by the U.S. Government.

## Data availability

All data are made available with the publication. All data and Jupyter notebooks are also stored on Github ([https://github.com/cljdevitre/2023\\_Kilauea-rapid-response-simulation](https://github.com/cljdevitre/2023_Kilauea-rapid-response-simulation)). The Github repository will be archived on Zenodo upon acceptance.

## References

1. Gansecki, C. *et al.* The tangled tale of Kīlauea’s 2018 eruption as told by geochemical monitoring. *Science* **366**, eaaz0147 (2019).
2. Re, G., Corsaro, R. A., D’Orlando, C. & Pompilio, M. Petrological monitoring of active volcanoes: A review of existing procedures to achieve best practices and operative protocols during eruptions. *J. Volcanol. Geotherm. Res.* **419**, 107365 (2021).
3. Pankhurst, M. J. *et al.* Rapid response petrology for the opening eruptive phase of the 2021 Cumbre Vieja eruption, La Palma, Canary Islands. *Volcanica* **5**, 1–10 (2022).
4. Wieser, P. E., Kent, A., Till, C. & Abers, G. Geophysical and Geochemical Constraints on Magma Storage Depths along the Cascade Arc: Knowns and Unknowns. *Geochemistry, Geophys. Geosystems* (In Press). Preprint at <https://doi.org/10.31223/X5KX00> (2023).

- 306 5. Wieser, P. E. *et al.* Barometers Behaving Badly I: Assessing the Influence of Analytical and Experimental  
307 Uncertainty on Clinopyroxene Thermobarometry Calculations at Crustal Conditions. *J. Petrol.* **64**, egac126  
308 (2023).
- 309 6. Wieser, P. E., Kent, A. J. R. & Till, C. B. Barometers Behaving Badly II: a Critical Evaluation of Cpx-Only  
310 and Cpx-Liq Thermobarometry in Variably-Hydrous Arc Magmas. *J. Petrol.* **64**, egad050 (2023).
- 311 7. Anderson, K. R. & Poland, M. P. Bayesian estimation of magma supply, storage, and eruption rates using a  
312 multiphysical volcano model: Kīlauea Volcano, 2000–2012. *Earth Planet. Sci. Lett.* **447**, 161–171 (2016).
- 313 8. Baker, S. & Amelung, F. Top-down inflation and deflation at the summit of Kīlauea Volcano, Hawai‘i  
314 observed with InSAR. *J. Geophys. Res. Solid Earth* **117**, (2012).
- 315 9. Dayton, K. *et al.* Deep magma storage during the 2021 La Palma eruption. *Sci. Adv.* **9**, eade7641 (2023).
- 316 10. DeVitre, C. L. & Wieser, P. Reliability of Raman analyses of CO<sub>2</sub>-rich fluid inclusions as a rapid barometer  
317 at Kīlauea. Preprint at <https://doi.org/10.31223/X5XD4F> (2023).
- 318 11. DeVitre, C. L., Allison, C. M. & Gazel, E. A high-precision CO<sub>2</sub> densimeter for Raman spectroscopy using a  
319 Fluid Density Calibration Apparatus. *Chem. Geol.* **584**, 120522 (2021).
- 320 12. Anderson, K. R. *et al.* Magma reservoir failure and the onset of caldera collapse at Kīlauea Volcano in 2018.  
321 *Science* **366**, eaaz1822 (2019).
- 322 13. Lerner, A. H. *et al.* The petrologic and degassing behavior of sulfur and other magmatic volatiles from the  
323 2018 eruption of Kīlauea, Hawai‘i: melt concentrations, magma storage depths, and magma recycling. *Bull.*  
324 *Volcanol.* **83**, 1–32 (2021).
- 325 14. Wieser, P. E. *et al.* Reconstructing Magma Storage Depths for the 2018 Kīlauean Eruption From Melt Inclusion  
326 CO<sub>2</sub> Contents: The Importance of Vapor Bubbles. *Geochem. Geophys. Geosystems* **22**, e2020GC009364  
327 (2021).



- 328 15. Welsch, B., Faure, F., Famin, V., Baronnet, A. & Bachèlery, P. Dendritic Crystallization: A Single Process for  
329 all the Textures of Olivine in Basalts? *J. Petrol.* **54**, 539–574 (2013).
- 330 16. Mourey, A. J., Shea, T., Costa, F., Shiro, B. & Longman, R. J. Years of magma intrusion primed Kīlauea  
331 Volcano (Hawai’i) for the 2018 eruption: evidence from olivine diffusion chronometry and monitoring data.  
332 *Bull. Volcanol.* **85**, 18 (2023).
- 333 17. Ryan, M. P. The elasticity and contractancy of Hawaiian olivine tholeiite, and its role in the stability and  
334 structural evolution of sub-caldera magma reservoirs and rift systems. In *Volcanism in Hawaii. US Geol Surv*  
335 *Prof Pap* **1350**, 1395–1447 (1987).
- 336 18. Wieser, P. E. & DeVitre, C. L. DiadFit: An Open-SourcePython3 Tool for Peak fitting of Raman Data from  
337 silicate melts and CO2 fluids. Preprint at <https://doi.org/10.31223/X5CQ1F> (2023).
- 338 19. Burke, E. A. J. Raman microspectrometry of fluid inclusions. *Lithos* **55**, 139–158 (2001).
- 339 20. Span, R. & Wagner, W. A new equation of state for carbon dioxide covering the fluid region from the triple-  
340 point temperature to 1100 K at pressures up to 800 MPa. *J. Phys. Chem. Ref. Data* **25**, 1509–1596 (1996).
- 341 21. Jarosewich, E., Nelen, J. A. & Norberg, J. A. Reference samples for electron microprobe analysis. *Geostand.*  
342 *NewsL.* **4**, 43–47 (1980).
- 343 22. Armstrong, J. T. Accurate quantitative analysis of oxygen and nitrogen with a W/Si multilayer crystal.  
344 *Microbeam Anal.* 301–304 (1988).
- 345

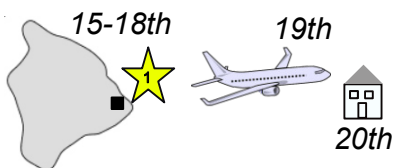
Sample erupted  
10th Sept



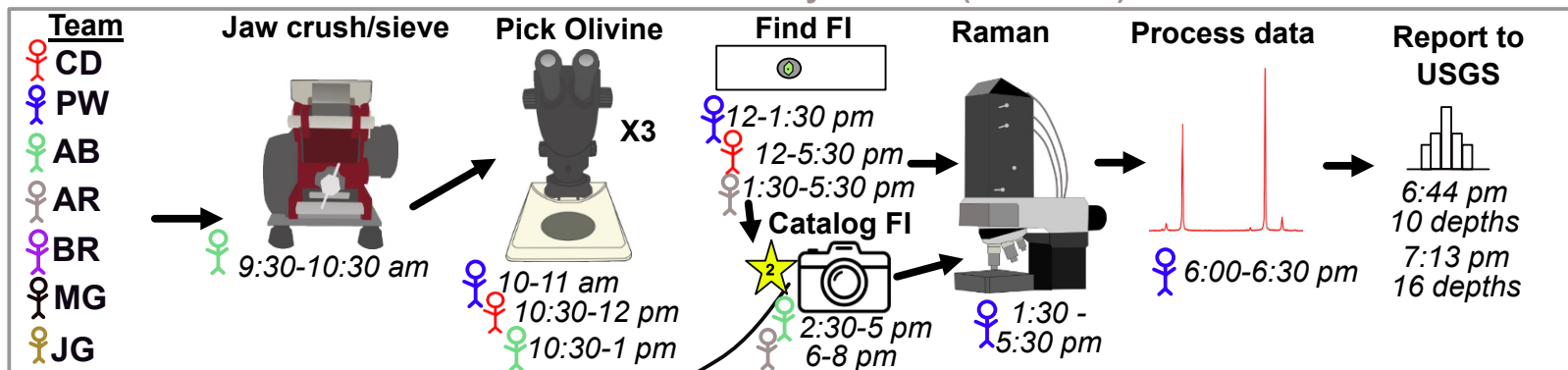
Sample collected  
12th Sept



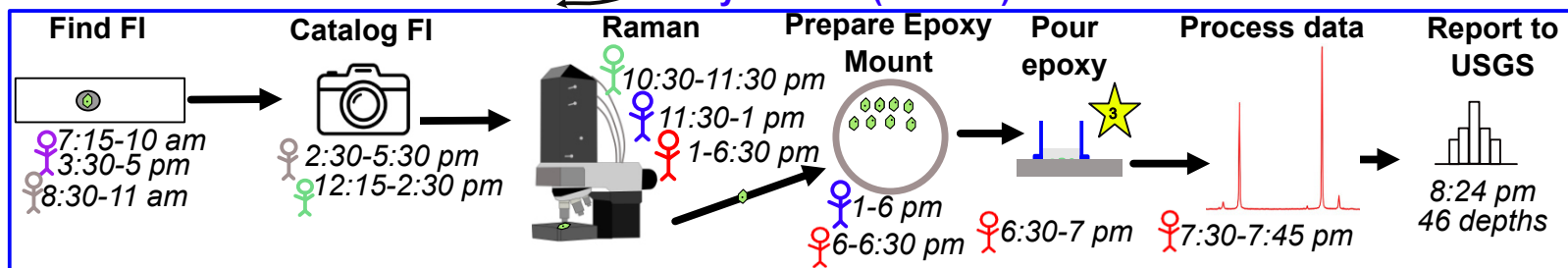
Sample taken to Hilo  
(15th Sept)



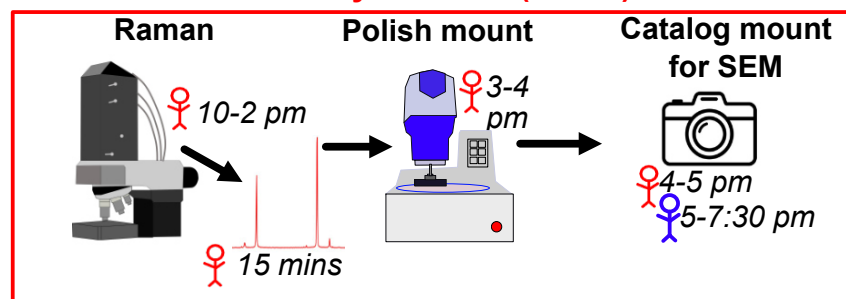
### Day 1 - 20th (~26.5 hrs)



### Day 2 - 21st (~23 hrs)



### Day 3 - 22nd (~9hrs)



### Day 4- 23rd (10.5 hrs analysis, 14 hrs report)

